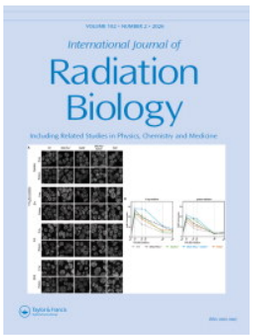

International Journal of Radiation Biology

ISSN: 0955-3002 (Print) 1362-3095 (Online) Journal homepage: www.tandfonline.com/journals/irab20

Radiobiological investigations of a [^{212}Pb]Pb-carbonic anhydrase IX-targeting small-molecule ligand in renal cell carcinoma and colorectal cancer models

Sandra K. Kristiansen, Kirill Shubin, Asta Zubrienė, Daumantas Matulis, Nurtene Dernjani, Petras Juzenas, Øyvind S. Bruland & Asta Juzeniene

To cite this article: Sandra K. Kristiansen, Kirill Shubin, Asta Zubrienė, Daumantas Matulis, Nurtene Dernjani, Petras Juzenas, Øyvind S. Bruland & Asta Juzeniene (2026) Radiobiological investigations of a [^{212}Pb]Pb-carbonic anhydrase IX-targeting small-molecule ligand in renal cell carcinoma and colorectal cancer models, International Journal of Radiation Biology, 102:2, 127-137, DOI: 10.1080/09553002.2025.2595630

To link to this article: https://doi.org/10.1080/09553002.2025.2595630

INTERNATIONAL JOURNAL OF RADIATION BIOLOGY
2026, VOL. 102, NO. 2, 127–137
https://doi.org/10.1080/09553002.2025.2595630

Taylor & Francis
Taylor & Francis Group

ORIGINAL ARTICLE

Radiobiological investigations of a [^{212}Pb]Pb-carbonic anhydrase IX-targeting small-molecule ligand in renal cell carcinoma and colorectal cancer models

Sandra K. Kristiansen[a,b], Kirill Shubin[c], Asta Zubrienė[d], Daumantas Matulis[d], Nurtene Dernjani[a,e], Petras Juzenas[a], Øyvind S. Bruland[f,g] and Asta Juzeniene[a,b]

[a]Department of Radiation Biology, Institute for Cancer Research, The Norwegian Radium Hospital, Oslo University Hospital, Oslo, Norway; [b]Department of Physics, University of Oslo, Oslo, Norway; [c]Latvian Institute of Organic Synthesis, Riga, Latvia; [d]Department of Biothermodynamics and Drug Design, Institute of Biotechnology, Life Sciences Center, Vilnius University, Vilnius, Lithuania; [e]Department of Molecular Biology, Norwegian University of Life Science, Ås, Norway; [f]Department of Medical Oncology & Radiotherapy, Division of Cancer Medicine, The Norwegian Radium Hospital, Oslo University Hospital, Oslo, Norway; [g]Faculty of Medicine, Institute of Clinical Medicine, University of Oslo, Oslo, Norway

ABSTRACT

Purpose: Carbonic anhydrase IX (CAIX), overexpressed in multiple cancers but limited in normal tissue, is a promising target for radionuclide therapy. This study evaluates [^{212}Pb]Pb-MKV-509, a novel DOTA-conjugated small-molecule ligand, for CAIX-targeted alpha therapy in preclinical renal carcinoma (SK-RC-52) and colorectal (HT-29) cancer models.

Materials and methods: [^{212}Pb]Pb-MKV-509 was assessed for radiochemical purity and stability. Binding assays determined receptor density and dissociation constants. Clonogenic survival, flow cytometry (viability, DNA damage, cell cycle), and spheroid assays (cross-sectional area, doubling time) evaluated biological responses. An in vivo biodistribution study was performed in SK-RC-52 xenograft-bearing mice, with and without carbonic anhydrase pre-blocking using acetazolamide.

Results: [^{212}Pb]Pb-MKV-509 exhibited high radiochemical purity (>96%) and stability for up to 48 h. Specific binding was higher in SK-RC-52 than in HT-29 cells. Treatment induced activity-dependent clonogenic inhibition, G2/M arrest, and DNA damage, with greater sensitivity observed in SK-RC-52 cells. Clonogenic survival was reduced by 50% at 3.4 kBq/mL (SK-RC-52) and 7.1 kBq/mL (HT-29). In spheroid models, 2.5–5.0 kBq/mL delayed growth and prolonged doubling time, indicating cross-fire effects. The biodistribution study revealed significant tumor uptake (4.7%IA/g at 2 h), along with high gastrointestinal accumulation. Pretreatment with acetazolamide partially reduced uptake in the stomach and intestines as well as in the tumor.

Conclusions: These findings highlight the potential of CAIX-targeted alpha therapy. CAIX expression and receptor density impact binding affinity and therapeutic response. The study demonstrates the importance of 3D tumor models in evaluating alpha-particle cross-fire effects. Further ligand optimization is warranted to enhance tumor specificity and minimize off-target uptake.

ARTICLE HISTORY
Received 12 June 2025
Revised 25 September 2025
Accepted 17 November 2025

KEYWORDS
Carbonic anhydrase IX; targeted alpha-therapy; lead-212; radiobiology; hypoxia

Background

Hypoxia is a hallmark of many solid tumors, triggering increased glycolysis to generate energy and essential metabolic precursors, leading to the accumulation of acidic metabolites and a subsequent drop in pH (Lau et al. 2017). To survive under these conditions, tumors activate hypoxia-inducible factors (HIFs) that upregulate pH-regulating genes, including the cell surface glycoprotein carbonic anhydrase IX (CAIX) (Lau et al. 2017). CAIX plays a critical role in cellular adaptation to hypoxia and contributes to cancer progression through both its enzymatic and noncatalytic functions (Dudutienė et al. 2014; Ronca and Supuran 2024). High CAIX expression is linked to tumor aggressiveness, metastasis, therapy resistance, and poor prognosis (Ronca and Supuran 2024). Low expression in normal tissues and widespread overexpression in various cancers, including clear cell renal carcinoma (ccRCC) and colorectal cancer (CRC), make CAIX an attractive theranostic target (Massière et al. 2024; Ronca and Supuran 2024).

Several CAIX-targeting agents have been developed, ranging from monoclonal antibodies to small-molecule ligands (Lau et al. 2017). Antibodies, such as cG250, labeled with beta-emitters like ^{177}Lu, have shown potential in metastatic ccRCC (Muselaers et al. 2016), but their clinical utility is limited by poor tumor penetration, prolonged circulation, and a higher risk of hematologic toxicity (Muselaers et al. 2016). In contrast, small-molecule ligands offer faster pharmacokinetics, improved tumor penetration, lower immunogenicity, and simpler, more cost-effective production (Lau et al. 2017; Rowe et al. 2023; Wang et al. 2025). Recent

CONTACT Asta Juzeniene astaj@ous-hf.no Department of Radiation Biology, Institute for Cancer Research, The Norwegian Radium Hospital, Oslo University Hospital, Oslo, Norway.

Supplemental data for this article can be accessed online at https://doi.org/10.1080/09553002.2025.2595630.

studies using CAIX-targeting peptides have shown favorable tumor-specific uptake, tolerability, and rapid systemic elimination in ccRCC patients (Hofman et al. 2024), in addition to high antitumor efficacy in CRC and ccRCC xenograft models (Massière et al. 2024).

Beta-emitters rely on oxygen to generate reactive oxygen species, making them less effective in hypoxic tumors. In contrast, alpha-particle therapies with high linear energy transfer (LET) induce complex DNA double-strand breaks primarily via direct ionization, and remain effective under hypoxic conditions (Wenker et al. 2025). Additionally, the short range of alpha particles enables selective eradication of malignant cells and micrometastases while sparing surrounding healthy tissue, a key advantage in targeted radionuclide therapy (TRT) (Hatcher-Lamarre et al. 2021). Promising results have been reported with the alpha-emitting radioimmunoconjugate [^{225}Ac]Ac-cG250 in ccRCC; however, concerns remain regarding activity-dependent renal toxicity, distribution of radioactive daughters (Merkx et al. 2022), and the limited global availability of ^{225}Ac (De Kruijff et al. 2015).

Alternatively, ^{212}Pb is a beta-emitting radionuclide that acts as an in vivo generator of alpha-emitting daughters, either ^{212}Bi or ^{212}Po. Each decay chain results in the emission of a single high-energy alpha particle, delivering localized cytotoxic radiation at the tumor site. With a half-life of 10.6 h, ^{212}Pb is compatible with the pharmacokinetics of small-molecule ligands and is more readily available than ^{225}Ac (Merkx et al. 2022). To our knowledge, no prior studies have evaluated ^{212}Pb-labeled CAIX-targeting conjugates for TRT or investigated their cellular effects. This preclinical study investigates the therapeutic potential of [^{212}Pb]Pb-MKV-509, a novel DOTA-conjugated derivative of the CAIX-targeting small-molecule inhibitor VD11-4-2 (Dudutienė et al. 2014; Kazokaitė et al. 2017; Matulienė et al. 2022; Vaškevičius et al. 2025b). Special emphasis is placed on receptor quantification, radiocytotoxicity in both 2D and 3D cell culture models, and in vivo distribution.

Material and methods

Radioligand preparation, quality control, and stability

Lead-212 was extracted from a ^{228}Th-based generator as previously described (Li et al. 2023). The activity of ^{212}Pb was quantified using a Capintec CRC-25R dose calibrator (Capintec Inc., Ramsey, NJ). A Hidex automatic gamma counter (Hidex Oy, Turku, Finland) or a Cobra gamma counter (Packard Instrument Company, Downers Grove, IL) was used to measure ^{212}Pb activity (50-120 keV) and to indirectly quantify ^{212}Bi via its daughter ^{208}Tl (500–800 keV) activities (Napoli et al. 2020). All measurements were performed at least 2 h post radiolabeling to ensure transient equilibrium with decay products.

The DOTA-conjugated CAIX inhibitor MKV-509 (purity >95%, Figures S1–S3) was custom-synthesized by the Latvian Institute of Organic Synthesis (Riga, Latvia). The quinoline-based Fibroblast Activation Protein (FAP)-targeted tracer FAPI-46 (#HY-137331, MedChemExpress EU, Germany) was used as a negative control (Figures S4 and S5). MKV-509 was dissolved in DMSO, and FAPI-46 in metal-free water. Each ligand was mixed with a 10% solution of 5 M sodium acetate (NaAc) in 0.1 M HCl and preheated at 95 °C (450 rpm, 5 min) using a Thermomixer (Eppendorf, Hamburg, Germany). Lead-212 was then added to achieve a molar activity of 1.7–2.3 MBq/nmol for MKV-509, and 1.3–1.8 MBq/nmol for FAPI-46. The pH was adjusted to 5–6 using 5 M NaAc, followed by incubation at 95 °C (450 rpm, 15 min). Radiochemical purity (RCP) was assessed using instant thin-layer chromatography (iTLC, Tec-Control, Biodex Medical Systems, Shirley, NY). Only preparations with RCP ≥97% were used in subsequent experiments.

The stability of [^{212}Pb]Pb-MKV-509 was evaluated by incubating the compound in phosphate-buffered saline (PBS), fetal bovine serum (FBS), or complete cultivation medium (1:1) for up to 48 h at room temperature. Stability was assessed using iTLC.

Cell lines

The SK-RC-52 ccRCC cell line was obtained from the Memorial Sloan Kettering Cancer Center (MSK, New York, USA), and the HT-29 CRC cell line from ATCC (ATCC® HTB-38™, Manassas, VA, USA). SK-RC-52 cells were cultured in RPMI-1640 medium (Sigma-Aldrich, Norway AS, Oslo), while HT-29 cells were maintained in McCoy's 5a (Modified) Medium (Thermo Fisher Scientific, Frankfurt, Germany) supplemented with 10% FBS (VWR, Oslo, Norway), 100 units/mL penicillin, and 100 μg/mL streptomycin (Sigma-Aldrich). Cells were maintained at 37 °C in a humidified atmosphere containing 5% CO_2.

Evaluation of surface protein expression

Cell surface CAIX expression was assessed by flow cytometry using the monoclonal antibody G250 (V6 Anti-Human CA9 (GirentuximabRencarex), #B839201, Abinvivo). Cells (5×10^5) were suspended in 100 µL of flow buffer (Dulbecco's PBS with 0.5% bovine serum albumin (BSA), Sigma-Aldrich) and incubated with primary antibody (50 µg/mL) for 1 h at 4 °C with gentle agitation. After three washes (2 mL flow buffer, centrifuged at 260 × g for 5 min), cells were incubated with secondary antibody, Alexa Fluor® 647 AffiniPure™ Goat Anti-Human IgG (H + L) (10 µg/mL; #109-605-088, Jackson ImmunoResearch Europe) for 30 min at 4 °C in the dark. Following final washes, cells were resuspended in 200 µL flow buffer and analyzed using a Cytoflex S flow cytometer with CytExpert 2.0 software (Beckman Coulter, Inc., Brea, CA). Data were analyzed using FlowJo software version 10.7.1 (FlowJo, LLC, Ashland, OR).

Binding studies

Saturation binding assays were performed by incubating 1×10^6 cells in 0.2 mL PBS with 0.5% BSA with increasing concentrations of [^{212}Pb]Pb-MKV-509 (0.6–150 nM) for 1 h

at 37 °C (150 rpm). Nonspecific binding was determined by preincubating cells with acetazolamide (45 nM; #A601, Sigma-Aldrich Norway AS) for 15 min to block carbonic anhydrases prior to radioligand addition. The activities (CPM) were measured in the gamma counter before (total added activity) and after incubation, followed by three washes with PBS containing 0.5% BSA (cell-bound activity). Specific binding was calculated as the percentage of added activity minus nonspecific binding (activity on blocked cells). Internalized activity was assessed by incubating cells with stripping buffer (50 mM glycine and 100 mM NaCl, pH 2.8) for 10 min at room temperature (150 rpm), followed by three washes. Internalization was calculated in the same manner as specific activity. The number of specifically bound ligands per cell, the maximum binding sites per cell (B_{max}), and the equilibrium dissociation constant (K_d) were determined using nonlinear regression (SigmaPlot 15.0, Systat Software, Inc., San Jose, CA, USA) based on a one-site binding saturation.

Detection of cell cycle progression and DNA damage

Cells ($0.35–1 \times 10^6$) were seeded 24 h prior to treatment with [^{212}Pb]Pb-MKV-509 (6.25–50 kBq/mL) for 1 h at 37 °C. After incubation, the radioligand-containing medium was replaced with fresh medium, and cells were cultured for 1, 3, and 6 days under standard conditions. At each time point, cells were harvested for further analysis. Cells were stained with fixable viability dye FVD-eFluor450 (Invitrogen, Thermo Fisher Scientific, Oslo, Norway) for 1 h on ice with gentle agitation, fixed in 100% methanol (Sigma-Aldrich Norway AS), and washed with PBS containing 0.2% Tween-20 (PBST; Sigma-Aldrich Norway AS). Cells were incubated with anti-pγH2AX (1 μg/mL; #05-636, Merck Millipore, Darmstadt, Germany) and RNase A (0.4 mg/mL; #12091021, PureLink, Thermo Fisher Scientific) in PBST with 2% FBS for 1 h at room temperature in the dark. After washing, cells were incubated with FITC-conjugated goat antimouse antibody (2 μg/mL; #F0479, Agilent Technologies, Santa Clara, CA, USA) in PBST with 2% FBS for 30 min at room temperature in the dark, then washed, and resuspended in propidium iodide (PI, 10 μg/mL) in PBST. Samples were analyzed using the Cytoflex S flow cytometer, and data analysis was performed using the FlowJo software. Cell cycle analysis was performed utilizing the Watson (pragmatic) model.

Clonogenic assay

The reproductive capacity of [^{212}Pb]Pb-MKV-509 and [^{212}Pb]-FAPI-46 treated cells was investigated using a clonogenic assay. Cells were seeded in T25 flasks, treated with [^{212}Pb]Pb-MKV-509 or [^{212}Pb]Pb-FAPI-46 (1.6–50 kBq/mL) for 1 h at 37 °C the following day, and then washed and incubated under standard conditions for 14 days. Cells were fixed with 96% ethanol and stained with 0.4% methylene blue (Thermo Fisher Scientific, Waltham, MA, USA). Colonies containing ≥50 cells were counted manually. Survival fractions were calculated relative to untreated controls. For [^{212}Pb]Pb-MKV-509, survival data were modeled using a double exponential decay equation ($f = ae^{-bx} + ce^{-dx}$, where x is the activity (kBq/mL) and a, b, c, and d are constants). For [^{212}Pb]Pb-FAPI-46, survival data were modeled using a single exponential decay equation ($f = ae^{-bx}$, where x is the activity and a and b are constants). Curve fitting and inhibitory activity concentration (IC) calculations were performed using SigmaPlot 15.0 software.

Spheroid treatment

Multicellular tumor spheroids were generated using the liquid-overlay technique (Carlsson and Yuhas 1984). Briefly, 500 cells were seeded in 100 μL culture medium per well in 96-well flat-bottom plates precoated with 50 μL of 1.5% (w/v) agarose (Sigma-Aldrich) in PBS. Plates were centrifuged at 470 × g for 15 min and incubated (37 °C, 5% CO_2). Spheroids were treated 4–5 days (defined as day 0) after seeding by incubating with [^{212}Pb]Pb-MKV-509 (0.5–80 kBq/mL) for 1 h. Following treatment, the unbound radioligand was removed by six sequential washes with fresh medium. Each treatment group had 3–6 technical replicates. Spheroids were imaged on days 0, 3, 7, 14, and 17 posttreatment using a Carl Zeiss Axiovert 200 Inverted Motorized Microscope with bright field, 4× objective. On day 17, viability was determined using PI (2 mg/mL) and fluorescein diacetate (FDA) (5 mg/mL; #F738, Sigma-Aldrich) staining. Cross-sectional area (μm^2) was determined in the AxioVision Rel. 4.8 imaging software (Carl Zeiss Microscopy GmbH, Germany). Spheroid doubling time was calculated during the exponential growth phase using exponential growth regression (single-term, two-parameter equation) in SigmaPlot 15.0.

Animal xenograft studies

A pilot in vivo study was conducted using eight male Hsd: Athymic Nude-Foxn1^{nu} mice bred at the Department of Comparative Medicine, Norwegian Radium Hospital (Oslo University Hospital, Oslo, Norway). All procedures were approved by the Institutional Committee on Research Animal Care and the Norwegian Food Safety Authority (Brumunddal, Norway, approval: FOTS ID 30148). The study adhered to the Interdisciplinary Principles and Guidelines for the Use of Animals in Research, Marketing, and Education (New York Academy of Sciences, New York, NY, USA) and complied with the EU Directive 2010/63/EU on animal experiments. Mice were housed under specific pathogen-free conditions, with up to five per cage, under controlled temperature (24 °C) and humidity (60%). The mice had access to food and water ad libitum. At the start of the study, the mice were 9 weeks old and weighed between 31 and 36 g.

For tumor engraftment, mice were subcutaneously injected in both flanks with 5×10^6 SK-RC-52 cells per flank in RPMI-1640 medium mixed in a 1:1 ratio with Matrigel Matrix (Corning Inc., Corning, NY, USA), in a total volume of 200 μL per injection. Tumor growth was monitored, and biodistribution studies were conducted when tumors reached 150–1000 mm^3.

Biodistribution studies

Mice were injected intravenously via the tail vein with 83 kBq (0.048 nmol) of [^{212}Pb]Pb-MKV-509 with or without prior oral administration of acetazolamide in saline (~30 min prior, 10 mg/kg, 100 µL). Blood samples were collected via cardiac puncture after 2 or 24 h under gas anesthesia (~3.5% sevoflurane in oxygen at 0.5 L/min; Baxter, IL, USA). Following euthanasia by cervical dislocation, various organs were harvested. Radioactivity and tissue weight were measured using a HIDEX gamma counter. The decay-corrected percentage of the injected activity per gram of tissue (%IA/g) was calculated using injection standards.

Statistical analyses

All statistical analyses were conducted using SigmaPlot 15.0 software. Data were tested for normality and equal variance using the Shapiro–Wilk and Brown–Forsythe tests, respectively.

Group comparisons were conducted using one-way Analysis of variance (ANOVA), with Holm–Sidak post hoc corrections. For groups where assumptions for parametric testing were not met, nonparametric tests were employed. Statistical significance was determined at a p-value of <.05. Results are presented as mean ± standard deviation (SD).

Results

Stability of [^{212}Pb]Pb-MKV-509

The stability of [^{212}Pb]Pb-MKV-509 in FBS, PBS, and complete culture medium was assessed by iTLC at 1, 4, 24, and 48 h postradiolabeling. The RCP remained above 90% at all time points, indicating high stability of the radioligand in different solutions (Table 1). At the time of radiolabeling ($t = 0$), the RCP was 98.7 ± 1.2% and 94.1 ± 4.7% for [^{212}Pb]Pb-MKV-509 and [^{212}Bi]Bi-MKV-509, respectively.

The release of ^{212}Bi following the decay of [^{212}Pb]Pb-MKV-509 was quantified by comparing the RCP of the daughter [^{212}Bi]Bi-MKV-509 to that of the parent conjugate. At 1 h postradiolabeling, the RCP of [^{212}Bi]Bi-MKV-509 was ~80% across all tested solutions. Due to the short half-life of [^{212}Bi]Bi (~1 h), its activity dropped to 6.4% after 4 h. At this point, the RCP decreased to about 74%, reflecting the combined effect of decay of initial [^{212}Bi]Bi-MKV-509 and the ingrowth of [^{212}Bi]Bi-MKV-509 from the decay of [^{212}Pb]Pb-MKV-509. From 4 to 48 h, the RCP of [^{212}Bi]Bi-MKV-509 declined from 74% to 71% (Table 1). Across all tested solutions, the estimated release of ^{212}Bi ranged from 20.1% to 23.3% during the 4- to 48-h incubation period, respectively.

Cell surface CAIX expression

Flow cytometry analysis revealed that SK-RC-52 cells displayed a bimodal CAIX expression, indicating the presence of two distinct populations with different antigen density (Figure 1). In contrast, HT-29 cells exhibited a more unified CAIX-positive population (Figure 1).

Radioligand binding and cytotoxic effects in monolayer cultures

SK-RC-52 cells exhibited significantly higher binding and internalization of [^{212}Pb]Pb-MKV-509 compared to HT-29 cells (Figure 2(A)), consistent with a fourfold higher antigen density (Figure 2(B) and Table 2). Despite differences in receptor expression, both cell lines displayed similar K_d values (~19 nM), indicating high-affinity ligand–receptor interactions under saturating conditions (Table 2).

Clonogenic assays demonstrated an activity-dependent inhibition of colony formation, with a plateau effect at the highest activities (Figure 2(C)). SK-RC-52 cells were more sensitive to treatment compared to HT-29, as reflected by lower survival fractions and IC values (Table 2). The negative control, [^{212}Pb]Pb-FAPI-46, induced an exponential reduction in clonogenic survival, resulting in approximately a 30% reduction at 50 kBq/mL in both cell lines (Figure 2(C)).

Cell cycle alterations and DNA damage following [^{212}Pb]Pb-MKV-509 treatment

Flow cytometry analysis revealed an activity-dependent accumulation of cells in the G2/M phase in both cell lines at day 1 posttreatment (Figure 3(A)). In SK-RC-52 cells, the G2/M fraction increased from ~14% to 25–54% following treatment with 6–50 kBq/mL, accompanied by a significant reduction in S-phase from ~31% to 23–14%. In HT-29 cells, the G2/M fraction increased from ~10% to 15–23%, while S-phase distribution remained largely unchanged (Table S1).

DNA damage was confirmed by γH2AX staining, which showed a ~2-fold increase in SK-RC-52 cells at day 3 posttreatment, and a ~1.5-fold increase in HT-29 cells at day 1 following exposure to 50 kBq/mL (Figure 3(B)). In SK-RC-52,

Table 1. Radiochemical purity (RCP) of [^{212}Pb]Pb-MKV-509 and [^{212}Bi]Bi-MKV-509 diluted 1:1 in PBS, FBS, or complete culture medium up to 48 h.

	RCP (%)					
	PBS		FBS		Complete medium	
Incubation time (h)	^{212}Pb	^{212}Bi	^{212}Pb	^{212}Bi	^{212}Pb	^{212}Bi
1	96.0 ± 0.5	80.4 ± 1.8	96.3 ± 0.7	81.4 ± 1.4	96.1 ± 0.7	80.5 ± 2.2
4	94.8 ± 0.1	73.8 ± 3.8	95.6 ± 0.7	76.4 ± 5.1	95.1 ± 0.3	75.4 ± 3.0
24	94.2 ± 0.5	73.0 ± 2.2	95.3 ± 0.4	76.9 ± 2.3	95.2 ± 0.3	76.0 ± 3.0
48	92.7 ± 2.1	71.1 ± 2.7	93.1 ± 2.7	71.4 ± 4.3	93.9 ± 1.6	72.7 ± 4.0

Data are presented as mean ± SD, $n = 3$.

a significant difference in γH2AX levels was detected between all activities at 6 days posttreatment. However, no significant differences in γH2AX levels were detected between the days within each activity group. HT-29 cells showed a significant increase in γH2AX signal between 6 kBq/mL and 50 kBq/mL at day 3. A significant reduction in DNA damage was also observed at all tested activities from day 1 to day 6, indicating progressive DNA repair over time.

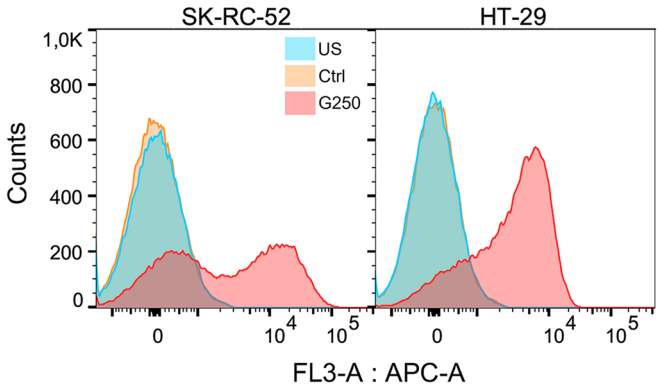

Figure 1. Cell surface expression of CAIX. Flow cytometry analysis of SK-RC-52 and HT-29 cells stained with Girentuximab (G250) followed by Alexa Fluor® 647 AffiniPure™ Goat Anti-Human IgG (H+L) secondary antibody. Unstained cells (US), cells stained with secondary antibody (Ctrl).

Growth dynamics of multicellular spheroids

Treatment with [^{212}Pb]Pb-MKV-509 significantly delayed spheroid growth in both SK-RC-52 and HT-29 models (Figure 4). Untreated HT-29 spheroids disintegrated over time, limiting the experiment to 17 days. In SK-RC-52 spheroids, 0.56 kBq/mL significantly reduced spheroid growth by day 3, but spheroids resumed expansion after 14 days (Figure 4(A), Table S2). The treatment caused a significant activity-dependent increase in doubling time (Figure 4(A)). Viability staining (FDA/PI) showed mostly viable spheroids at all activities on day 17. Increasing activity from 5 to 80 kBq/mL did not enhance the effect, as no significant differences in cross-sectional area were observed by the end of the experiment (Table S2).

HT-29 spheroids exhibited lower sensitivity to [^{212}Pb]Pb-MKV-509 treatment compared to SK-RC-52 (Figure 4). Among the tested activities, 5 kBq/mL was the only activity that significantly prolonged doubling time and reduced spheroid size at days 7 and 14 (Figure 4(A,B)). Interestingly, treatment with 0.56 kBq/mL resulted in a transient increase in spheroid size on day 7 compared to the untreated control (Table S2). At activities above 5 kBq/mL, HT-29 spheroids showed widespread loss of viability and were primarily composed of dead cells (Figure 4(B)).

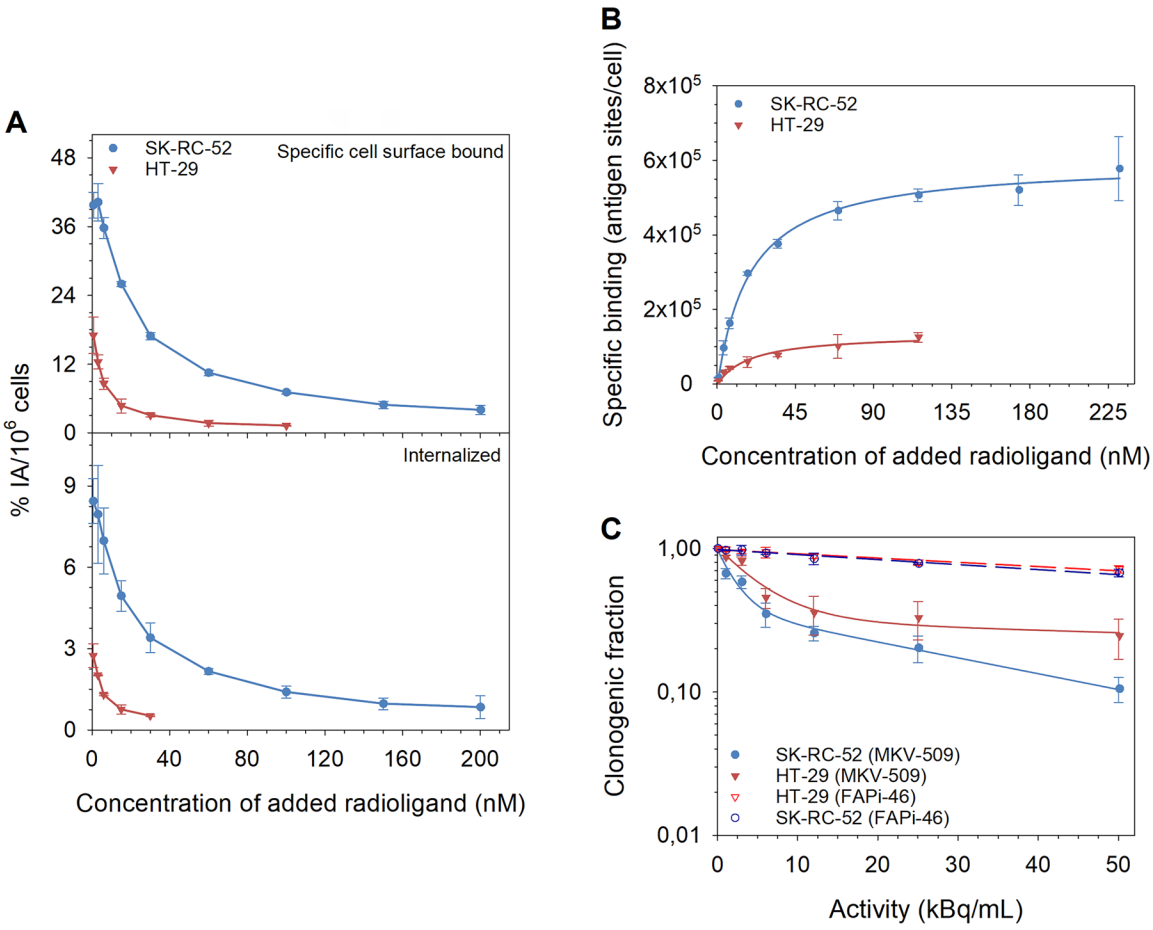

Figure 2. (A) Specific binding and internalization of [^{212}Pb]Pb-MKV-509 in SK-RC-52 and HT-29 cells, expressed as percentage of total added. (B) Saturation binding curves showing specific binding of [^{212}Pb]Pb-MKV-509 to CAIX antigen sites per cell in SK-RC-52 and HT-29 cells, plotted against ligand concentration (nM). Data are presented as mean ± SD, $n = 2$. Curves were fitted using nonlinear regression with a one site saturation equation in SigmaPlot 15 (solid lines). (C) Inhibition of colony formation in SK-RC-52 and HT-29 cells following a 1 h incubation with [^{212}Pb]Pb-MKV-509 compared to untreated control cells, with results shown as mean ± SD, $n = 3$-4. Curves (solid lines) were generated in SigmaPlot 15 using the bi-exponential model. Curves generated from the negative control, [^{212}Pb]Pb-FAPI-46 (dotted lines), were fitted using a single exponential model ($n = 2$).

In vivo biodistribution of [^{212}Pb]Pb-MKV-509

The biodistribution study in SK-RC-52 xenograft-bearing mice revealed tumor uptake of 4.7%IA/g at 2 h, which decreased to 2.2%IA/g by 24 h (Figure 5 and Table S3). Notably, high uptake was observed in the small intestine (8.7%IA/g), large intestine (7.5%IA/g), lungs (8.3%IA/g), and stomach (28.6%IA/g). Most tissues exhibited a tenfold reduction in activity by 24 h, except for the stomach (11.1%IA/g), which retained levels comparable to the tumor. Acetazolamide pretreatment significantly reduced off-target uptake, particularly in the stomach and intestines; however, it also lowered tumor uptake (1.1%IA/g) (Figure 5 and Table S3).

Table 2. Binding parameters and radiocytotoxic potency of [^{212}Pb]Pb-MKV-509 in SK-RC-52 and HT-29 cells.

Cell line	B_{max} (antigens/cell)	K_d (nM)	IC_{50} (kBq/mL)
SK-RC-52	596 212 ± 11 266	19 ± 2	3.4 ± 0.9
HT-29	134 342 ± 12 636	19 ± 6	7.1 ± 1.5

The total receptor density per cell (B_{max}), equilibrium dissociation constant (K_d), and the inhibitory activity concentration required to reduce colony formation by 50% (IC_{50}).

Discussion

This study presents the first preclinical evaluation of a ^{212}Pb-labeled small-molecule radioligand targeting CAIX in preclinical models of solid tumors. [^{212}Pb]Pb-MKV-509 exhibited high stability, tumor-specific uptake, and antitumor effects across monolayer and spheroid cultures. These results underscore the potential of targeted alpha therapy using a small-molecule ligand to induce DNA damage, disrupt cell cycle progression, and inhibit growth in both monolayer and 3D spheroid models.

The clonogenic assays revealed a biphasic response to increasing activities of [^{212}Pb]Pb-MKV-509 for both cell lines, characterized by an initial decrease in survival followed by a plateau at higher activities. The negative control [^{212}Pb]Pb-FAPI-46 demonstrated a linear effect in both cell lines, indicating that the observed biphasic response was receptor-mediated. Oversaturation could cause receptors to become occupied, and increasing the activity (i.e., radioligand concentration) would not induce a higher response, as the redundant radioligands are washed away after 1 h. SK-RC-52 cells demonstrated significantly higher specific binding, internalization, and antigen density per cell

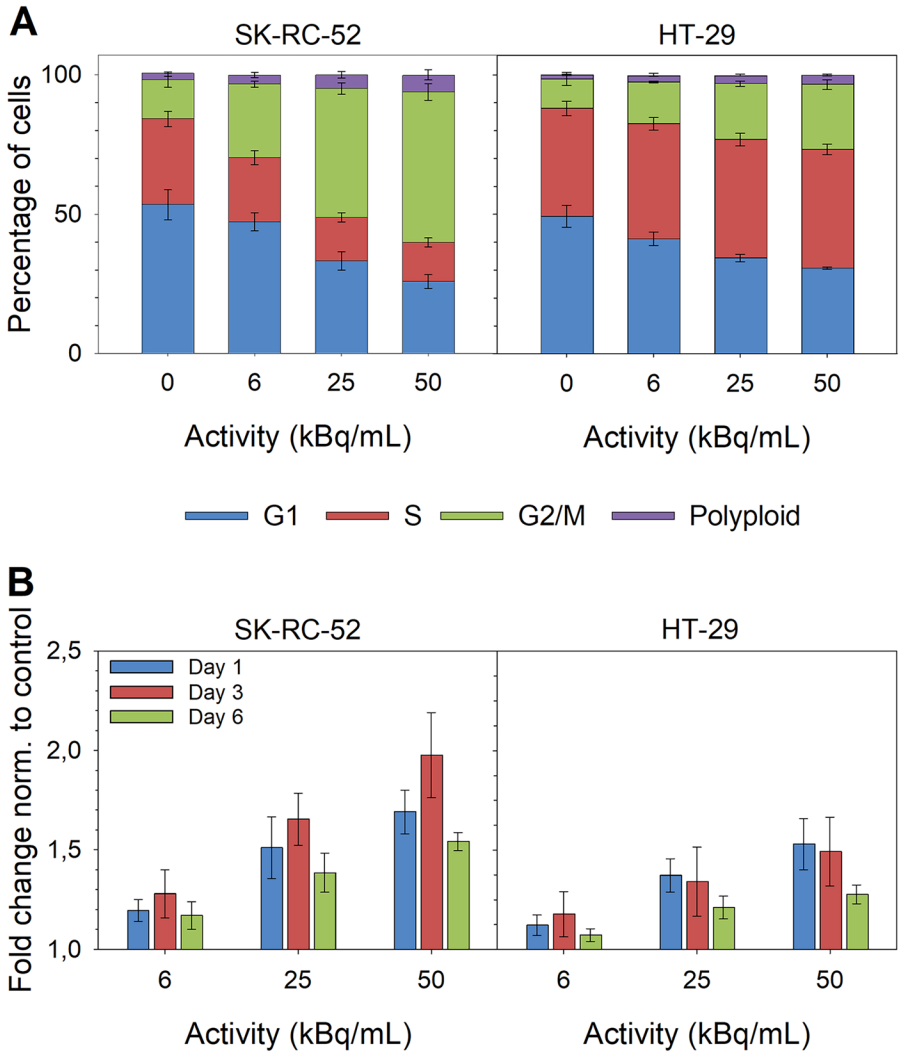

Figure 3. Cell cycle disruptions and DNA damage induction following [^{212}Pb]Pb-MKV-509 treatment. (A) Cell cycle distribution 1 day post-treatment and (B) γH2AX expression in SK-RC-52 and HT-29 cells after 1 h exposure to [^{212}Pb]Pb-MKV-509. Cells were fixed in methanol, stained with primary- and secondary antibodies, and counterstained with propidium iodide at 1-, 3-, and 6 days post-treatment. Data are presented as mean ± SD, $n = 3$.

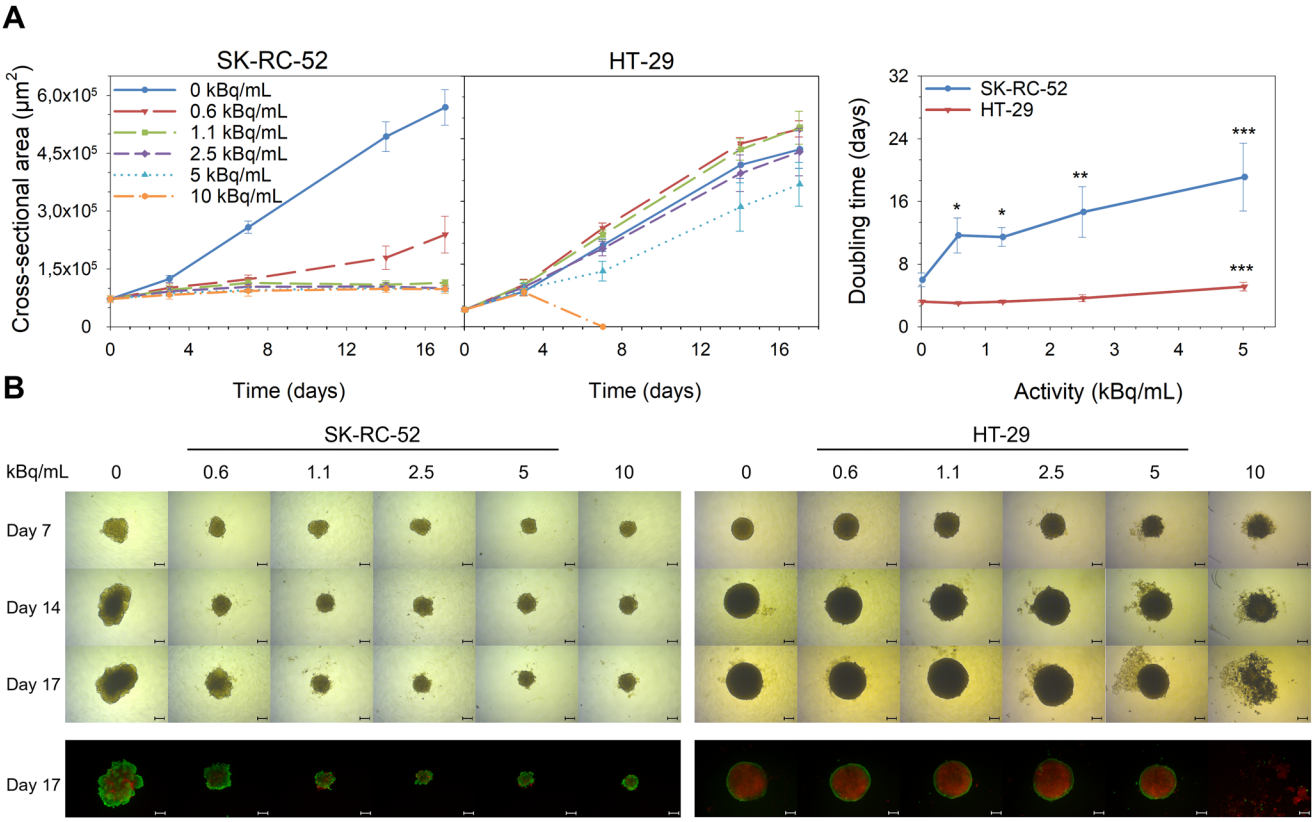

Figure 4. Growth inhibition in SK-RC-52 and HT-29 spheroids following [^{212}Pb]Pb-MKV-509 treatment. (A) Cross-sectional area (μm^2) and doubling time of SK-RC-52 and HT-29 spheroids at different days after 1 h incubation with [^{212}Pb]Pb-MKV-509. Data are presented as mean ± SD, $n = 3$. (B) Microscope images 4x magnification (200 μm scalebar) were captured from day 0 to day 17 post-treatment. Viability staining with fluorescein diacetate (FDA) and propidium iodide (PI) was performed on day 17 to differentiate viable from non-viable cells.

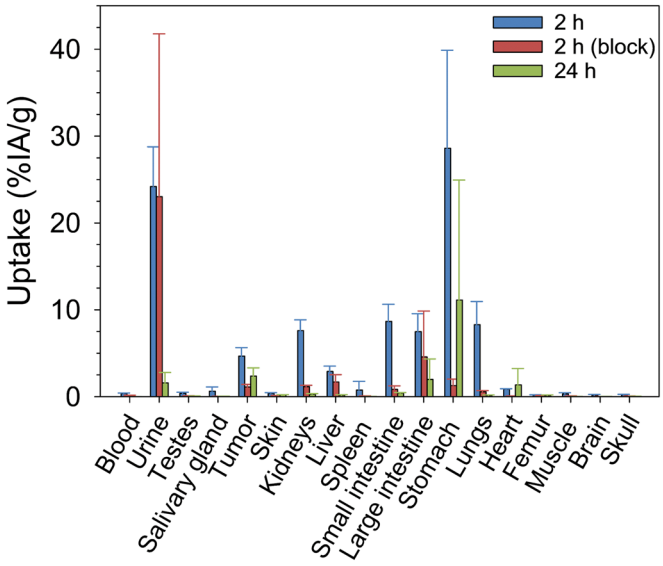

Figure 5. Tissue uptake of [^{212}Pb]Pb-MKV-509 in SK-RC-52 xenograft-bearing mice. Biodistribution is shown as percent of injected activity per gram of tissue (%IA/g) at 2 h ($n = 4$) and 24 h ($n = 2$) postinjection. Two mice were given acetazolamide (10 mg/kg, oral administration) 30 min prior to radioligand administration (2 h, block). Data are presented as mean ± SD.

compared to HT-29 cells. The maximum internalization was ~8% of total added activity (~22% of specifically bound fraction) at the lowest radioligand concentration tested (Figure 2(A)). Previous studies have shown that CAIX-ligand complexes do not undergo efficient internalization, at least with small-molecule ligands (Krall et al. 2014). Consistently, VD11-4-2 predominantly exhibited cell-surface binding (Matulienė et al. 2022), and minimal internalization was also reported for the dicyclic peptide DPI-4452 in HT-29 cells (Massière et al. 2024). The SK-RC-52 cells were also more sensitive to radioligand treatment, showing a lower IC_{50} value. These results suggest that cells with higher CAIX receptor density sustain greater alpha-induced damage, while those with low or no ligand binding exhibit a more gradual response. Further analysis correlating CAIX expression with radiation response could clarify this relationship.

Flow cytometry analysis confirmed radiation-induced DNA damage, with the highest γH2AX levels detected at 1 and 3 days posttreatment in HT-29 and SK-RC-52 cells, respectively. By day 6, the DNA damage decreased in HT-29 cells, possibly due to activation of DNA repair mechanisms. Additionally, heavily damaged cells may have undergone cell death, indicating selective survival of less-damaged cells (Figure S6). Radiation-induced DNA damage has been reported to cause G2/M-phase arrest (Hwang and Muschel 1998). Indeed, the cell cycle distribution following ^{212}Pb exposure showed a substantial G2/M arrest, consistent with previous findings of alpha radiation effects (Vallon et al. 2012; Yong et al. 2012, 2013). This arrest was transient, peaking at day 1 posttreatment, followed by an activity- and time-dependent recovery (Figures S7 and S8), indicating that cells may have either repaired the damage prompting the arrest or bypassed the cell cycle inhibition through

alternative mechanisms. Similar findings have been reported previously with alpha radiation (Palayoor et al. 1993; Vallon et al. 2012).

The multicellular tumor spheroid models displayed increased treatment sensitivity, consistent with observations from other ^{212}Pb-labeled radiopharmaceuticals investigated, suggesting the influence of a 3D cross-fire effect mediated by alpha-particle emissions (Boyd et al. 2001; Pekeč et al. 2023; Lindland and Juzeniene 2025; Liukaityte et al. 2025). Alpha particles travel approximately 40–80 μm (about three to five cell diameters), enabling deposition of energy and induction of damage in neighboring cells as well as the target cells (Song et al. 2012; Staudacher et al. 2014). The lack of an increased effect with increasing activities observed in SK-RC-52 spheroids may be due to oversaturation or reduced receptor accessibility and limited diffusion of the radioligand within the spheroid (Judmann et al. 2024). In HT-29 spheroids, treatment disrupted cell-cell interactions, resulting in a less compact peripheral structure and eventual spheroid disintegration at ≥5 kBq/mL. This phenomenon, previously described for this cell line (Thakuri et al. 2019), is characterized by a distinctive ruffled surface (Figures 4 and S9). After exposure to low activities of [^{212}Pb]Pb-MKV-509, HT-29 spheroids displayed an increased cross-sectional area compared to controls, suggesting reduced compactness. This may result from compromised core integrity and weakened cell-cell adhesions or enhanced cellular migration (Bulin et al. 2019). The intact spheroids remained viable throughout the experiment, consistent with the minimal apoptosis and cell death detected in 2D monolayer via flow cytometry (Figure S8). In contrast, disintegrated HT-29 spheroids were largely nonviable, likely due to a combination of high radiation exposure and the loss of cell-cell contacts, leading to cellular dissociation (Figure 4) (Baek et al. 2016).

Both cell lines displayed CAIX expression, but not all cells were CAIX-positive. SK-RC-52 cells demonstrated a bimodal distribution, whereas HT-29 cells showed a more uniform positive population. Still, SK-RC-52 cells demonstrated higher specific binding and radiosensitivity in all in vitro assays compared to HT-29 cells, suggesting a higher functional receptor density and greater cell-intrinsic susceptibility (Kleinendorst et al. 2024). HT-29, which exhibited 'high CAIX positivity but lower receptor density' per cell, showed greater resistance to radiation-induced growth inhibition, potentially linked to their p53-null status (Gao et al. 2009; Wang et al. 2018). These results indicate that CAIX expression levels did not directly correlate with ligand binding or sensitivity. This discrepancy suggests that functional receptor density and intrinsic cellular factors may influence ligand binding and therapeutic response. Similar discrepancies between protein expression and the uptake and sensitivity of radioligands have previously been observed in tumor models (Lindeman et al. 2023). These findings suggest that receptor density and functional binding, rather than just CAIX expression, influence the therapeutic response.

The biodistribution study revealed rapid tumor uptake of [^{212}Pb]Pb-MKV-509 (4.7%IA/g at 2 h). This uptake is comparable to that reported for other small CAIX-targeting molecules (Askoxylakis et al. 2010; Wang et al. 2025). Small-molecule ligands are predominantly eliminated via the renal pathway, resulting in an initial peak in kidney uptake (Vegt et al. 2010). By 24 h, [^{212}Pb]Pb-MKV-509 levels in kidneys had dropped by more than 90% compared to the 2 h time point, suggesting efficient clearance. High uptake in the stomach, intestines, and lungs suggests off-target binding. Significant stomach uptake of CAIX-targeted radioconjugates has been reported previously, consistent with CAIX expression in this organ (Ivanov et al. 2001; Yang et al. 2019; Kulterer et al. 2021; Zhu et al. 2023; Hofman et al. 2024; Lou et al. 2024; Massière et al. 2024; Horii et al. 2025; Müller et al. 2025; Wang et al. 2025). High uptake in the lungs is of particular interest, since human lung tissue does not express CAIX (Ivanov et al. 2001). In contrast, murine lungs do express CAIX, which may account for the observed binding of MKV-509. Similar lung uptake has been demonstrated previously (Yang et al. 2019; Zhu et al. 2023; Müller et al. 2025). Uptake in both stomach and lung may also result from interactions with other carbonic anhydrase isoforms, and improving ligand specificity could help to reduce this off-target accumulation (Imtaiyaz Hassan et al. 2013; Vaškevičius et al. 2025a).

Acetazolamide pretreatment reduced off-target accumulation but also decreased tumor uptake, highlighting the challenge of balancing specificity and efficacy (Figure 5). This underscores the importance of carefully evaluating and managing the risk of off-target effects when targeting CAIX to ensure both treatment efficacy and safety. Therapeutic studies were not pursued due to the substantial off-target uptake. Beyond ligand optimization, several parameters could be adjusted to improve efficacy, including radionuclide selection, fractionated dosing, or combination approaches (Kleinendorst et al. 2024; Wang et al. 2025). The short range of alpha particles may limit efficacy in antigen-heterogenous tumors, as the cross-fire effects are inferior to those of beta emitters (Aghevlian et al. 2017). In this context, careful selection of the radionuclide payload is important, since beta emitters or tandem alpha/beta combinations may compensate for heterogeneous target expression through enhanced cross-fire (Aghevlian et al. 2017; Khreish et al. 2020). However, long-lived radionuclides such as ^{177}Lu are not well suited for fast-clearing CAIX-targeting small molecules, as their pharmacokinetics may limit tumor retention and thereby reduce tumor-absorbed dose (Merkx et al. 2022; Müller et al. 2025).

[^{212}Pb]Pb-MKV-509 exhibited high RCP and stability in vitro, consistent with previous findings from our group, showing that both DOTA-conjugated PSMA-617 and TCMC-conjugated PSMA-targeting ligands maintain RCPs above 90% after 48 h and with comparable radiolytic stability (Stenberg et al. 2020). The low uptake in the femur and skull (Figure 5) confirmed in vitro stability, as free ^{212}Pb is known to accumulate in bones (Chapeau et al. 2023). Across all tested solutions, the consistent loss of approximately one-fifth of ^{212}Bi from the [^{212}Bi]Bi-MKV-509 was observed following β^- decay (Table 1). These results align with previous studies on DOTA-based chelation, in which 36% of [^{212}Bi]Bi-DOTA complexes break up following beta decays due to internal conversion processes that impart enough kinetic and electronic excitation to disrupt the daughter's chelate (Mirzadeh

et al. 1993). Studies have shown that TCMC is a better-suited chelator for ^{212}Pb (Meredith et al. 2014).

These findings support further refinement of CAIX-targeting alpha therapy, particularly through modification of linker length and lipophilicity, improvement of isoform selectivity, evaluation of alternative chelators, and exploration of combination therapies to maximize efficacy while minimizing off-target effects (Benešová et al. 2016; Holik et al. 2022). Future studies will include direct comparisons of ^{212}Pb and ^{177}Lu payloads, alpha/beta tandem regimens, fractionated dosing with mass-dose and molar-activity optimization, and combination approaches with DNA damage response modulators or immunotherapies.

Conclusion

This study establishes [^{212}Pb]Pb-MKV-509 as a promising CAIX-targeted alpha therapy for solid tumors, providing critical radiobiological insights from preclinical models. Our findings confirm that a short-lived alpha-emitting radionuclide can effectively induce DNA damage, trigger G2/M arrest, and inhibit cell growth, offering an alternative to ^{225}Ac- and ^{177}Lu-based therapies. The observed heterogeneous responses in SK-RC-52 and HT-29 models underscore the need to consider receptor distribution and cellular sensitivity when optimizing treatment strategies. Additionally, our data provide evidence on alpha-particle cross-fire effects in 3D spheroid models, where ligand diffusion and receptor saturation may limit activity escalation benefits. Biodistribution studies revealed significant off-target uptake, emphasizing the need for more selective CAIX ligands. Future efforts should focus on developing ligands with improved tumor targeting and minimal accumulation in healthy tissues.

Acknowledgments

The authors acknowledge Elisabeth Wiig, Li-Wei Ma, Andrius Kleinauskas, and Rugile Liukaityte for technical assistance with ^{212}Pb harvesting, cell preparations, and flow cytometry.

Disclosure statement

The authors report no conflict of interest.

Author contributions

The authors S.K.K. and A.J. contributed to the study conception and design. Experimental execution and analysis were performed by S.K.K., A.J., and N.D. S.K.K. and A.J. wrote the first draft of the manuscript, and all authors commented on previous versions of the manuscript. All authors read and approved the final manuscript.

Funding

This work was supported by RadForsk (the TARACAN project) and the European Union's Horizon 2020 research and innovation program under grant agreement No. 101008571 (PRISMAP).

Notes on contributors

Sandra Kvarsvik Kristiansen holds a master's degree and is a Ph.D. student in the Targeted Alpha Therapy group at the Department of Radiation Biology, Oslo University Hospital. Her research is part of the TARACAN project, funded by RadForsk, which focuses on the development of novel targeted alpha-emitting radiopharmaceuticals for the treatment of metastases of solid tumors.

Dr. Kirill Shubin is a Principal Scientist at the Latvian Institute of Organic Synthesis, specializing in medicinal chemistry and radiopharmaceutical development. His research focuses on the synthesis and characterization of novel small-molecule ligands and radiolabeled compounds for targeted cancer therapy and molecular imaging.

Dr. Asta Zubrienė is a senior researcher at the Department of Biothermodynamics and Drug Design, Institute of Biotechnology, Vilnius University. Her research focuses on protein-ligand interactions, drug design, biophysical methods, enzyme inhibition, and protein stability.

Prof. Daumantas Matulis is the Head of the Department of Biothermodynamics and Drug Design of the Life Sciences Center at Vilnius University, where he leads research on protein biophysics, drug discovery, and molecular interactions. His expertise lies in thermodynamic and structural characterization of protein-ligand binding, with applications in oncology and infectious diseases.

Nurtene Dernjani holds a bachelor's degree and works as a laboratory technician at the Department of Radiation Biology, Oslo University Hospital, where she contributes to experimental research in molecular and radiation biology. Her academic and professional interests focus on the intersection of biotechnology, cancer research, and therapeutic innovation.

Dr. Petras Juzenas is a senior researcher at the Department of Radiation Biology, Oslo University Hospital, and a member of the PROTONICs project group. His research focuses on the advancement of photodynamic therapy, radiation therapy, and proton therapy, with a particular emphasis on the development of novel photosensitizers and radiosensitizers for cancer treatment. Dr. Juzenas is also an expert in flow cytometry, which he applies to investigate cellular responses to therapeutic interventions.

Prof. Øyvind S. Bruland is a clinical oncologist and a leading expert in targeted radionuclide therapy and bone sarcoma treatment. He played a pivotal role in the clinical development of radium-223 dichloride (Xofigo®), the first alpha-emitting radiopharmaceutical approved for cancer therapy. His research bridges basic radiobiology, translational oncology, and clinical trials, with a focus on improving outcomes for patients with cancer metastases. Prof. Bruland's work has significantly shaped the field of nuclear medicine and continues to influence the development of novel radiotherapeutics.

Dr. Asta Juzeniene is the group leader of the Targeted Alpha Therapy group at the Department of Radiation Biology, Oslo University Hospital, and an associate professor at the University of Oslo. Her research is dedicated to the development, optimization, and preclinical evaluation of targeted radionuclide therapies, with a particular emphasis on alpha-emitting isotopes for the treatment of cancer. Dr. Juzeniene leads multidisciplinary projects that bridge radiobiology, nuclear medicine, and translational oncology, aiming to advance precision medicine approaches in cancer therapy.

ORCID

Sandra K. Kristiansen http://orcid.org/0009-0009-9548-8056
Kirill Shubin http://orcid.org/0000-0002-9542-9170
Asta Zubrienė http://orcid.org/0000-0001-5996-1883
Daumantas Matulis http://orcid.org/0000-0002-6178-6276
Nurtene Dernjani http://orcid.org/0009-0005-8157-6128
Petras Juzenas http://orcid.org/0000-0002-0114-903X
Øyvind S. Bruland http://orcid.org/0000-0003-1631-3733
Asta Juzeniene http://orcid.org/0000-0001-9426-0062

References

Aghevlian S, Boyle AJ, Reilly RM. 2017. Radioimmunotherapy of cancer with high linear energy transfer (LET) radiation delivered by radionuclides emitting α-particles or Auger electrons. Adv Drug Deliv Rev. 109:102–118. https://doi.org/10.1016/j.addr.2015.12.003

Askoxylakis V et al. 2010. A new peptide ligand for targeting human carbonic anhydrase IX, identified through the phage display technology. PLoS One. 5(12):e15962. https://doi.org/10.1371/journal.pone.0015962

Baek N, Seo OW, Kim M, Hulme J, An SS. 2016. Monitoring the effects of doxorubicin on 3D-spheroid tumor cells in real-time. Onco Targets Ther. 9:7207–7218. https://doi.org/10.2147/OTT.S112566

Benešová M et al. 2016. Linker modification strategies to control the prostate-specific membrane antigen (PSMA)-targeting and pharmacokinetic properties of DOTA-conjugated PSMA inhibitors. J Med Chem. 59(5):1761–1775. https://doi.org/10.1021/acs.jmedchem.5b01210

Boyd M et al. 2001. A gene therapy/targeted radiotherapy strategy for radiation cell kill by [^{131}I]meta-iodobenzylguanidine. J Gene Med. 3(2):165–172. https://doi.org/10.1002/1521-2254(2000)9999:9999<::AID-JGM158>3.0.CO;2-C

Bulin A-L, Broekgaarden M, Simeone D, Hasan T. 2019. Low dose photodynamic therapy harmonizes with radiation therapy to induce beneficial effects on pancreatic heterocellular spheroids. Oncotarget. 10(27):2625–2643. https://doi.org/10.18632/oncotarget.26780

Carlsson J, Yuhas JM. 1984. Liquid-overlay culture of cellular spheroids. Recent Results Cancer Res. 95:1–23. https://doi.org/10.1007/978-3-642-82340-4_1

Chapeau D et al. 2023. [^{212}Pb]Pb-eSOMA-01: a promising radioligand for targeted alpha therapy of neuroendocrine tumors. Pharmaceuticals. 16(7):985. https://doi.org/10.3390/ph16070985

De Kruijff RM, Wolterbeek HT, Denkova AG. 2015. A critical review of alpha radionuclide therapy—how to deal with recoiling daughters? Pharmaceuticals (Basel). 8(2):321–336. https://doi.org/10.3390/ph8020321

Dudutienė V et al. 2014. Discovery and characterization of novel selective inhibitors of carbonic anhydrase IX. J Med Chem. 57(22):9435–9446. https://doi.org/10.1021/jm501003k

Gao X et al. 2009. Radiosensitization of HT-29 cells and xenografts by the nitric oxide donor DETANONOate. J Surg Oncol. 100(2):149–158. https://doi.org/10.1002/jso.21318

Hatcher-Lamarre JL, Sanders VA, Rahman M, Cutler CS, Francesconi LC. 2021. Alpha emitting nuclides for targeted therapy. Nucl Med Biol. 92:228–240. https://doi.org/10.1016/j.nucmedbio.2020.08.004

Hofman MS et al. 2024. First-in-human safety, imaging, and dosimetry of a carbonic anhydrase IX-targeting peptide, [(^{68})Ga]Ga-DPI-4452, in patients with clear cell renal cell carcinoma. J Nucl Med. 65(5):740–743. https://doi.org/10.2967/jnumed.123.267175

Holik HA et al. 2022. The chemical scaffold of theranostic radiopharmaceuticals: radionuclide, bifunctional chelator, and pharmacokinetics modifying linker. Molecules. 27(10):3062. https://doi.org/10.3390/molecules27103062

Horii T et al. 2025. First-in-human phase 0 safety, imaging, pharmacokinetics, and dosimetry study of ^{64}Cu-PD-32766, a carbonic anhydrase IX (CAIX)-targeting peptide, in patients with clear cell renal cell carcinoma (ccRCC). J Clin Oncol. 43: TPS605. (5_suppl):TPS605.

Hwang A, Muschel RJ. 1998. Radiation and the G2 phase of the cell cycle. Radiat Res. 150(5 Suppl):S52–S59. https://doi.org/10.2307/3579808

Imtaiyaz Hassan M, Shajee B, Waheed A, Ahmad F, Sly WS. 2013. Structure, function and applications of carbonic anhydrase isozymes. Bioorg Med Chem. 21(6):1570–1582. https://doi.org/10.1016/j.bmc.2012.04.044

Ivanov S et al. 2001. Expression of hypoxia-inducible cell-surface transmembrane carbonic anhydrases in human cancer. Am J Pathol. 158(3):905–919. https://doi.org/10.1016/S0002-9440(10)64038-2

Judmann B et al. 2024. Are 3D tumor cell spheroids a utile system for the in vitro evaluation of diagnostic radiotracers? ACS Omega. 9(52):51349–51362. https://doi.org/10.1021/acsomega.4c08214

Kazokaitė J, Aspatwar A, Kairys V, Parkkila S, Matulis D. 2017. Fluorinated benzenesulfonamide anticancer inhibitors of carbonic anhydrase IX exhibit lower toxic effects on zebrafish embryonic development than ethoxzolamide. Drug Chem Toxicol. 40(3):309–319. https://doi.org/10.1080/01480545.2016.1223095

Khreish F et al. 2020. ^{225}Ac-PSMA-617/^{177}Lu-PSMA-617 tandem therapy of metastatic castration-resistant prostate cancer: pilot experience. Eur J Nucl Med Mol Imaging. 47(3):721–728. https://doi.org/10.1007/s00259-019-04612-0

Kleinendorst SC et al. 2024. Towards effective CAIX-targeted radionuclide and checkpoint inhibition combination therapy for advanced clear cell renal cell carcinoma. Theranostics. 14(9):3693–3707. https://doi.org/10.7150/thno.96944

Krall N et al. 2014. A small-molecule drug conjugate for the treatment of carbonic anhydrase IX expressing tumors. Angew Chem Int Ed Engl. 53(16):4231–4235. https://doi.org/10.1002/anie.201310709

Kulterer OC et al. 2021. A microdosing study with ^{99m}Tc-PHC-102 for the SPECT/CT imaging of primary and metastatic lesions in renal cell carcinoma patients. J Nucl Med. 62(3):360–365. https://doi.org/10.2967/jnumed.120.245530

Lau J, Lin KS, Bénard F. 2017. Past, present, and future: development of theranostic agents targeting carbonic anhydrase IX. Theranostics. 7(17):4322–4339. https://doi.org/10.7150/thno.21848

Li RG, Stenberg VY, Larsen RH. 2023. An experimental generator for production of high-purity ^{212}Pb for use in radiopharmaceuticals. J Nucl Med. 64(1):173–176. https://doi.org/10.2967/jnumed.122.264009

Lindeman SD et al. 2023. Fibroblast activation protein targeted radioligand therapy for treatment of solid tumors. J Nucl Med. 64(5):759–766. https://doi.org/10.2967/jnumed.122.264494

Lindland K, Juzeniene A. 2025. Cytotoxicity of ^{212}Pb-labeled anti-PTK7 antibody in 2D adherent and 3D multicellular bladder cancer models. EJNMMI Radiopharm Chem. 10(1):58. https://doi.org/10.1186/s41181-025-00382-3

Liukaityte R et al. 2025. Combination of PSMA targeting alpha-emitting radioligand [^{212}Pb]Pb-AB001 with BET bromodomain inhibitors in in vitro prostate cancer models. Med Oncol. 42(8):362. https://doi.org/10.1007/s12032-025-02925-9

Lou K et al. 2024. Value of [^{68}Ga]Ga-NYM046 PET/CT, in comparison with ^{18}F-FDG PET/CT, for diagnosis of clear cell renal cell carcinoma. J Nucl Med. 65(12):1884–1890. https://doi.org/10.2967/jnumed.124.267527

Massière F et al. 2024. Preclinical characterization of DPI-4452: a ^{68}Ga/^{177}Lu theranostic ligand for carbonic anhydrase IX. J Nucl Med. 65(5):761–767. https://doi.org/10.2967/jnumed.123.266309

Matulienė J et al. 2022. Picomolar fluorescent probes for compound affinity determination to carbonic anhydrase IX expressed in live cancer cells. Sci Rep. 12(1):17644. https://doi.org/10.1038/s41598-022-22436-1

Meredith RF et al. 2014. Pharmacokinetics and imaging of ^{212}Pb-TCMC-Trastuzumab after intraperitoneal administration in ovarian cancer patients. Cancer Biother Radiopharm. 29(1):12–17. https://doi.org/10.1089/cbr.2013.1531

Merkx RIJ et al. 2022. Carbonic anhydrase IX-targeted α-radionuclide therapy with ^{225}Ac inhibits tumor growth in a renal cell carcinoma model. Pharmaceuticals. 15(5):570. https://doi.org/10.3390/ph15050570

Mirzadeh S, Kumar K, Gansow OA. 1993. The chemical fate of ^{212}Bi-DOTA formed by β^- decay of ^{212}Pb(DOTA)$^{2-}$. Radiochimica Acta. 60(1):1–10. https://doi.org/10.1524/ract.1993.60.1.1

Muselaers CHJ et al. 2016. Phase 2 study of Lutetium 177-labeled anti-carbonic anhydrase IX monoclonal antibody Girentuximab in patients with advanced renal cell carcinoma. Eur Urol. 69(5):767–770. https://doi.org/10.1016/j.eururo.2015.11.033

Müller M et al. 2025. Small organic carbonic anhydrase IX ligands from DNA-encoded chemical libraries for tumor-targeted delivery of radionuclides. J Am Chem Soc. 147(21):18230–18239. https://doi.org/10.1021/jacs.5c05198

Napoli E et al. 2020. Calibration of sodium iodide detectors and reentrant ionization chambers for ^{212}Pb activity in different geometries by HPGe activity determined samples. Appl Radiat Isot. 166:109362. https://doi.org/10.1016/j.apradiso.2020.109362

Palayoor ST, Humm JL, Atcher RW, Hines JJ, Macklis RM. 1993. G2M arrest and apoptosis in murine T lymphoma cells following exposure to ^{212}Bi alpha particle irradiation. Nucl Med Biol. 20(6):795–805. https://doi.org/10.1016/0969-8051(93)90166-r

Pekeč T et al. 2023. Detecting radio- and chemoresistant cells in 3D cancer co-cultures using chromatin biomarkers. Sci Rep. 13(1):20662. https://doi.org/10.1038/s41598-023-47287-2

Ronca R, Supuran CT. 2024. Carbonic anhydrase IX: an atypical target for innovative therapies in cancer. Biochim Biophys Acta Rev Cancer. 1879(4):189120. https://doi.org/10.1016/j.bbcan.2024.189120

Rowe SP et al. 2023. Small molecules as vectors for radiopharmaceutical therapy. In: Bodei L, Lewis JS, Zeglis BM, editors. Radiopharmaceutical therapy. Springer. p. 349–367.

Song H, Senthamizhchelvan S, Hobbs RF, Sgouros G. 2012. Alpha particle emitter radiolabeled antibody for metastatic cancer: what can we learn from heavy ion beam radiobiology? Antibodies. 1(2):124–148. https://doi.org/10.3390/antib1020124

Staudacher AH, Bezak E, Borysenko A, Brown MP. 2014. Targeted α-therapy using ^{227}Th-APOMAB and cross-fire antitumour effects: preliminary in-vivo evaluation. Nucl Med Commun. 35(12):1284–1290. https://doi.org/10.1097/MNM.0000000000000199

Stenberg VY, Juzeniene A, Bruland ØS, Larsen RH. 2020. In situ generated ^{212}Pb-PSMA ligand in a ^{224}Ra-solution for dual targeting of prostate cancer sclerotic stroma and PSMA-positive cells. Curr Radiopharm. 13(2):130–141. https://doi.org/10.2174/1874471013666200511000532

Thakuri PS, Gupta M, Plaster M, Tavana H. 2019. Quantitative size-based analysis of tumor spheroids and responses to therapeutics. Assay Drug Dev Technol. 17(3):140–149. https://doi.org/10.1089/adt.2018.895

Vallon M et al. 2012. Enhanced efficacy of combined ^{213}Bi-DTPA-F3 and paclitaxel therapy of peritoneal carcinomatosis is mediated by enhanced induction of apoptosis and G2/M phase arrest. Eur J Nucl Med Mol Imaging. 39(12):1886–1897. https://doi.org/10.1007/s00259-012-2203-z

Vaškevičius A et al. 2025a. Design of rigid compounds to enhance selectivity for carbonic anhydrase IX. Chemistry. 31(18):e202404409. https://doi.org/10.1002/chem.202404409

Vaškevičius A et al. 2025b. Di-meta-substituted fluorinated benzenesulfonamides as potent and selective anticancer inhibitors of carbonic anhydrase IX and XII. J Med Chem. 68(17):18389–18406. https://doi.org/10.1021/acs.jmedchem.5c01142

Vegt E et al. 2010. Renal toxicity of radiolabeled peptides and antibody fragments: mechanisms, impact on radionuclide therapy, and strategies for prevention. J Nucl Med. 51(7):1049–1058. https://doi.org/10.2967/jnumed.110.075101

Wang J et al. 2025. [^{177}Lu]Lu-XYIMSR-01: a novel CAIX-targeted radiotherapeutic for enhanced treatment of malignant glioma. Bioconjug Chem. 36(3):588–596. https://doi.org/10.1021/acs.bioconjchem.5c00041

Wang Y et al. 2018. Radiosensitization by irinotecan is attributed to G2/M phase arrest, followed by enhanced apoptosis, probably through the ATM/Chk/Cdc25C/Cdc2 pathway in p53-mutant colorectal cancer cells. Int J Oncol. 53(4):1667–1680. https://doi.org/10.3892/ijo.2018.4514

Wenker STM et al. 2025. The potential of targeted radionuclide therapy to treat hypoxic tumor cells. Nucl Med Biol. 140-141:108971. https://doi.org/10.1016/j.nucmedbio.2024.108971

Yang X et al. 2019. Targeting CAIX with [^{64}Cu]XYIMSR-06 small molecular radiotracer enables noninvasive PET imaging of malignant glioma in U87 MG tumor cell xenograft mice. Mol Pharm. 16(4):1532–1540. https://doi.org/10.1021/acs.molpharmaceut.8b01210

Yong KJ, Milenic DE, Baidoo KE, Brechbiel MW. 2012. ^{212}Pb-radioimmunotherapy induces G(2) cell-cycle arrest and delays DNA damage repair in tumor xenografts in a model for disseminated intraperitoneal disease. Mol Cancer Ther. 11(3):639–648. https://doi.org/10.1158/1535-7163.MCT-11-0671

Yong KJ, Milenic DE, Baidoo KE, Brechbiel MW. 2013. Sensitization of tumor to ^{212}Pb radioimmunotherapy by Gemcitabine involves initial abrogation of G2 arrest and blocked DNA damage repair by interference with Rad51. Int J Radiat Oncol Biol Phys. 85(4):1119–1126. https://doi.org/10.1016/j.ijrobp.2012.09.015

Zhu W et al. 2023. Preclinical and pilot clinical evaluation of a small-molecule carbonic anhydrase IX targeting PET tracer in clear cell renal cell carcinoma. Eur J Nucl Med Mol Imaging. 50(10):3116–3125. https://doi.org/10.1007/s00259-023-06248-7